Monthly Notices of the ROYAL ASTRONOMICAL SOCIETY

MNRAS **452,** 3334–3345 (2015) doi:10.1093/mnras/stv1515

KIC 4768731: a bright long-period roAp star in the *Kepler* field

B. Smalley,[1⋆] E. Niemczura,[2] S. J. Murphy,[3,4] H. Lehmann,[5] D. W. Kurtz,[6] D. L. Holdsworth,[1] M. S. Cunha,[7] L. A. Balona,[8] M. Briquet,[9] H. Bruntt,[10] P. De Cat,[11] P. Lampens,[11] A. O. Thygesen[12] and K. Uytterhoeven[13,14]

[1]*Astrophysics Group, Lennard-Jones Laboratories, Keele University, Staffordshire ST5 5BG, UK*
[2]*Instytut Astronomiczny, Uniwersytet Wrocławski, Kopernika 11, PL-51-622 Wrocław, Poland*
[3]*Sydney Institute for Astronomy (SIfA), School of Physics, University of Sydney, NSW 2006, Australia*
[4]*Stellar Astrophysics Centre, Department of Physics and Astronomy, Aarhus University, DK-8000 Aarhus C, Denmark*
[5]*Thüringer Landessternwarte Tautenburg (TLS), Sternwarte 5, D-07778 Tautenburg, Germany*
[6]*Jeremiah Horrocks Institute, University of Central Lancashire, Preston PR1 2HE, UK*
[7]*Instituto de Astrofisica e Ciências do Espaço, Universidade do Porto, CAUP, Rua das Estrelas, P-4150-762 Porto, Portugal*
[8]*South African Astronomical Observatory, PO Box 9, Observatory 7935, Cape Town, South Africa*
[9]*Institut d'Astrophysique et de Géophysique, Université de Liège, Allée du 6 Août 19C, B-4000 Liège, Belgium*
[10]*Stellar Astrophysics Center, Department of Physics and Astronomy, Aarhus University, Ny Munkegade 120, DK-8000 Aarhus C, Denmark*
[11]*Royal observatory of Belgium, Ringlaan 3, B-1180 Brussel, Belgium*
[12]*Zentrum für Astronomie der Universität Heidelberg, Landessternwarte, Königstuhl 12, D-69117 Heidelberg, Germany*
[13]*Instituto de Astrofisica de Canarias, E-38205 La Laguna, Tenerife, Spain*
[14]*Departamento de Astrofisica, Universidad de La Laguna, E-38206 La Laguna, Tenerife, Spain*

Accepted 2015 July 6. Received 2015 July 3; in original form 2015 June 4

ABSTRACT

We report the identification of 61.45 d^{-1} (711.2 μHz) oscillations, with amplitudes of 62.6 μmag, in KIC 4768731 (HD 225914) using *Kepler* photometry. This relatively bright ($V = 9.17$) chemically peculiar star with spectral type A5 Vp SrCr(Eu) has previously been found to exhibit rotational modulation with a period of 5.21 d. Fourier analysis reveals a simple dipole pulsator with an amplitude that has remained stable over a 4-yr time span, but with a frequency that is variable. Analysis of high-resolution spectra yields stellar parameters of $T_{\rm eff} = 8100 \pm 200$ K, $\log g = 4.0 \pm 0.2$, [Fe/H] $= +0.31 \pm 0.24$ and $v \sin i = 14.8 \pm 1.6$ km s^{-1}. Line profile variations caused by rotation are also evident. Lines of Sr, Cr, Eu, Mg and Si are strongest when the star is brightest, while Y and Ba vary in antiphase with the other elements. The abundances of rare earth elements are only modestly enhanced compared to other roAp stars of similar $T_{\rm eff}$ and $\log g$. Radial velocities in the literature suggest a significant change over the past 30 yr, but the radial velocities presented here show no significant change over a period of 4 yr.

Key words: asteroseismology – techniques: photometric – stars: abundances – stars: chemically peculiar – stars: individual: KIC 4768731 – stars: oscillations.

1 INTRODUCTION

The chemically peculiar Ap stars are a spectroscopic subclass of A-type stars which exhibit strong enhancements of one or more elements, notably Cr, Eu, Si and Sr (Morgan 1933). Strong magnetic fields in Ap stars were found by Babcock (1947) and their presence appears ubiquitous with field strengths reaching several kilogauss (Donati & Landstreet 2009). As a group the Ap stars rotate more slowly than normal A-type stars due to magnetic breaking (Stępień 2000) and exhibit photometric and spectral variability due to inhomogeneous surface distributions of elemental abundances concentrated into spots by the magnetic field (Wolff 1983; Smith 1996).

The rapidly oscillating Ap (roAp) stars are a subset of the magnetic Ap stars (Kurtz 1982). These exhibit short-time-scale variations with periods between 5 and 25 min and amplitudes up to 0.01 mag. The roAp stars are relatively rare with 61 known to date (Table 1), compared to around 2000 known Ap stars (Renson & Manfroid 2009). Most have been found using ground-based photometry of already known Ap stars. Some, which do not exhibit photometric variations detectable from the ground, have been

⋆ E-mail: b.smalley@keele.ac.uk

Table 1. Catalogue of roAp stars. The first two columns are the HD number and other name if available. The effective temperature (K) is obtained from the Balmer line profiles when available. The luminosity, $L/L_{\odot}$ is obtained from $T_{\rm eff}$ and the surface gravity when available or from the radius. The projected rotational velocity, $v \sin i$ (km s^{-1}), is given. The averaged magnetic field, $\bar{B}$ (kG), from Bychkov, Bychkova & Madej (2009) are shown; values in italics are other measures of B. The rotation period, $P_{\rm rot}$ is determined from the light curve. A maximum of four pulsation frequencies is given.

HD	Name	log $T_{\rm eff}$ (K)	log L ($L_{\odot}$)	$v \sin i$ (km s^{-1})	$\bar{B}$ (kG)	$P_{\rm rot}$ (d)	Frequencies (μHz)	Reference
6532	AP Scl	3.914	1.22	30.0	0.40	1.944 973	2390.2, 2396.2, 2402.2, 2408.1,	Kurtz et al. (1996)
9289	BW Cet	3.907	1.08	10.5	0.07	8.55	1585.1, 1554.8, 1605.4	Kurtz, Martinez & Tripe (1994b)
12098	V988 Cas	3.892	0.88	–	1.00	5.460	2173.7, 2164.2, 2180.6, 2305.6	Girish et al. (2001)
12932	BN Cet	3.884	1.21	2.5	0.64	3.529 5?	1436.3	Martinez, Kurtz & van Wyk (1994)
19918	BT Hyi	3.899	1.06	3.0	0.21	–	1510.2, 3020.1, 1480.7	Martinez et al. (1995)
24355	J0353	3.916	–	–	–	13.859 611	2596	Holdsworth et al. (2014a)
24712	HR 1217	3.860	0.89		0.76	12.458 77	2619.5, 2653.0, 2687.6, 2721.0,	Kurtz et al. (2002)
42659	UV Lep	3.900	1.48	19.0	0.39	–	1735.5	Martinez, Kurtz & Ashley (1993b)
60435	V409 Car	3.910	1.14	10.8	0.30	7.6793	709.0, 761.4, 842.8, 939.7,	Matthews, Wehlau & Kurtz (1987)
69013		3.881	0.60	4.0	*4.8*	–	1485	Kochukhov et al. (2013)
75445		3.886	1.17	2.0	–	–	1850.0	Kochukhov et al. (2009)
80316	LX Hya	3.918	1.05	32.0	–	2.088 60	2246.1, 2251.6, 2257.2	Kurtz et al. (1997b)
83368	HR 3831	3.877	1.09	33.0	0.81	2.851 982	1415.8, 1419.9, 1424.0, 1428.0,	Kurtz et al. (1997a)
84041	AI Ant	3.916	–	25.0	0.48	3.69	1113.0, 1085.0, 1145.0	Martinez et al. (1993a)
86181	V437 Car	3.865	1.05	–	0.40	–	2688.0	Kurtz & Martinez (1994)
92499		3.875	1.14	3.3	*8.2*	–	1602	Elkin et al. (2010)
96237	TX Crt	3.892	0.88	6.0	*2.9*	–	1200	Kochukhov et al. (2013)
99563	XY Crt	3.886	1.10	28.0	0.57	–	1553.7, 1561.6, 1545.7, 1557.6,	Handler et al. (2006)
101065	V816 Cen	3.810	0.91	4.0	1.02	–	1372.8, 1381.5, 1314.6, 1379.8,	Mkrtichian et al. (2008)
115226		3.883	0.86	27.0	0.74	–	1534.0	Kochukhov et al. (2008b)
116114		3.870	1.32	2.2	1.92	–	790.0	Elkin et al. (2005a)
119027	LZ Hya	3.875	0.79	–	–	–	1953.7, 1940.5, 1913.4, 1887.9,	Martinez, Koen & Sullivan (1998a)
122970	PP Vir	3.840	0.82	4.2	0.19	3.877	1502.5, 1477.8, 1476.8, 1478.9	Handler et al. (2002)
128898	α Cir	3.875	1.03	13.5	0.32	4.4792	2442.6, 2265.4, 2341.8, 2366.5,	Kurtz et al. (1994a)
132205		3.892	0.77	9.5	*5.2*	–	2334	Kochukhov et al. (2013)
134214	HI Lib	3.858	0.85	2.6	0.46	248.00	2947.0, 2784.0, 2644.0, 2842.0,	Kurtz et al. (2007b)
137909	β CrB	3.908	1.37	3.5	0.51	–	967.0, 1062.0	Kochukhov et al. (2008a)
137949	33 Lib	3.869	1.09	3.0	2.14	–	2014.8, 4029.6, 1769.0	Kurtz, Elkin & Mathys (2005)
143487	–	3.845	0.0	1.5	*4.7*	–	1730	Kochukhov et al. (2013)
148593	–	3.894	0.78	5.0	*3.0*	–	1560	Kochukhov et al. (2013)
150562	V835 Ara	3.9:	–	1.5	*5.0*	–	1550.0	Martinez & Kurtz (1992)
151860	–	3.848	0.42	4.5	*2.5*	–	1355	Kochukhov et al. (2013)
154708		3.829	0.73	4.0	6.54	5.3666	2088.0	Kurtz et al. (2006)
161459	V834 Ara	–	–	–	1.76	–	1390.9	Martinez & Kauffmann (1990)
166473	V694 CrA	3.889	1.22	2.5	2.15	–	1833.0, 1886.0, 1928.0	Mathys, Kurtz & Elkin (2007)
176232	10 Aql	3.899	1.32	2.7	0.46	–	1447.9, 1396.9, 1427.1, 1366.2,	Huber et al. (2008)
177765	–	3.903	1.54	2.5	*3.6*	–	706	Alentiev et al. (2012)
185256	V4373 Sgr	–	–	6.2	0.71	–	1630.0	Kurtz & Martinez (1995)
190290	CK Oct	–	–	16.0	3.00	4.03	2270.0, 2230.0	Martinez, Kurtz & Kauffmann (1991)
193756	QR Tel	–	–	17.0	0.36	–	1284.0	Martinez & Kurtz (1990)
196470	AW Cap	–	–	–	1.47	–	1544.0	Martinez et al. (1990b)
201601	γ Equ	3.878	1.10	2.5	0.79	1785.70	1364.6, 1365.4, 1427.1, 1388.9,	Gruberbauer et al. (2008)
203932	BI Mic	–	–	4.7	0.25	–	1280.5, 2838.0, 2772.3, 2737.3	Martinez, Kurtz & Heller (1990a)
213637	MM Aqr	3.822	0.64	3.5	0.74	–	1452.3, 1410.9	Martinez et al. (1998b)
217522	BP Gru	3.816	0.85	2.7	0.69	–	1215.3, 1199.9, 2017.4	Kreidl et al. (1991)
218495	CN Tuc	3.888	1.10	16.0	0.77	–	2240.0	Martinez & Kurtz (1990)
218994	–	3.881	1.06	5.2	–	–	1170.0	González et al. (2008)
225914	KIC 4768731	3.888	1.33	14.8	*2.7*	5.205	711.2, 713.5, 709.0	This Work
	J0008	3.863	–	–	–	–	1739	Holdsworth et al. (2014a)
258048	J0629	3.820	–	–	–	–	1962	Holdsworth et al. (2014a)
	J0651	3.869	–	–	–	–	1532	Holdsworth et al. (2014a)
	J0855	3.892	–	–	–	3.09	2283	Holdsworth et al. (2014a)
97127	J1110	3.799	–	–	–	–	1234	Holdsworth et al. (2014a)
	J1430	3.851	–	–	–	–	2726	Holdsworth et al. (2014a)
	J1640	3.869	–	–	–	3.67	1758	Holdsworth et al. (2014a)
	KIC 7582608	3.940	1.13	<4	*3.1*	20.20	2103	Holdsworth et al. (2014b)
	J1921	3.792	–	–	–	–	1490	Holdsworth (2015)
	J1940	3.839	–	–	–	9.58	2042	Holdsworth et al. (2014a)
	KIC 8677585	3.863	0.80	4.2	–	–	1659.8, 1621.8, 1504.3, 1676.0	Balona et al. (2011a)
	KIC 10195926	3.869	1.61	21.0	–	5.684 59	972.6, 976.7, 974.6, 970.6	Kurtz et al. (2011)
	KIC 10483436	3.869	0.84	–	–	4.303	1353.0, 1347.6, 1358.4, 1508.9	Balona et al. (2011b)

found by spectroscopic studies looking for radial velocity (RV) variations (e.g. Kochukhov et al. 2002; Elkin et al. 2005b). 11 of the 61 known roAp stars have now been found using the SuperWASP archive with *V*-band amplitudes >0.5 mmag (Holdsworth et al. 2014a; Holdsworth 2015).

The launch of the *Kepler* spacecraft enabled the search for photometric oscillations with amplitudes well below those detectable from the ground. Seven stars previously classified as Ap stars were observed by *Kepler* to search for rapid oscillations, but only one was found to exhibit roAp pulsations (Balona et al. 2011a). Two further previously unknown Ap stars were identified from their pulsations and subsequent spectral analyses (Balona et al. 2011b; Kurtz et al. 2011). In the spectroscopic survey of 117 A and F stars observed by *Kepler*, Niemczura et al. (2015) identified one new Ap star (KIC 4768731), and re-classified two of the stars by Balona et al. (2011a) as not Ap (KIC 8750029 and KIC 9147002). All the *Kepler*-discovered roAp stars have oscillation amplitudes below 0.1 mmag, while one initially discovered by SuperWASP located in the *Kepler* field has an amplitude of over 1 mmag (Holdsworth et al. 2014b). The star discussed here, KIC 4768731, is brighter and has a lower pulsation frequency than the other known roAp stars in the *Kepler* field.

2 KIC 4768731

Prior to the *Kepler* mission, KIC 4768731 (HD 225914, BD +39 3919) was a rather anonymous $V = 9.17$ star (Høg et al. 2000) with a spectral type A7 (Cannon 1925). The star is part of the double system WDS 19484+3952 with a 12th magnitude star (KIC 4768748) at 12 arcsec (Mason et al. 2001). There has been very little change in separation or position angle over a period of 74 yr, suggesting that the two stars might be a common proper motion pair. Recent proper motion catalogues (Roeser, Demleitner & Schilbach 2010; Zacharias et al. 2013) are inconclusive in this regard, with both stars having proper motions that agree to within the error bars. Unfortunately, the *Hipparcos* parallax (Perryman & ESA 1997) of $\pi = 8.68 \pm 7.80$ mas is too uncertain to provide any meaningful distance constraint. The distance of ∼350 pc estimated from the stellar parameters (see Section 7) would imply a physical separation of at least 4000 au. However, the *Kepler* Input Catalog estimates $T_{\rm eff} = 4220$ K and $\log g = 1.55$ for the companion star, suggesting that this is a background K-type giant star. In Section 6, spectroscopic observations confirm this.

3 SPECTRAL CLASSIFICATION

KIC 4768731 was included in the sample of several hundred A- and F-type stars to be observed at high-resolution as part of the Kepler Asteroseismic Science Consortium (KASC) spectroscopic follow-up of stars with *Kepler* light curves (Niemczura et al. 2015). A spectrum of this star was taken on 2011 July 13 using the fibre-fed High Efficiency and Resolution Mercator Echelle Spectrograph (HERMES; Raskin et al. 2011). Fig. 1 presents the spectrum at classification resolution. This spectrum is a smoothed version of the high-resolution spectrum downgraded to a resolution of 1.8 Å to match that of the spectral standards.[1]

The H γ line and the strength of the metal lines in general match that of the A5V standard, but for an A5V star the Ca II K line is shallow and abnormally broad. This abnormal shape is due to abundance stratification within the star's atmosphere (see Section 7.3). The Ca I 4226 Å line, however, does not look abnormal. Sr II lines are particularly strong (see the 4077 and 4216 Å lines). Cr lines are also strong: the Cr II 4111 Å line that is blended in the redward core-wing boundary of H δ is pronounced, and this is confirmed with the Cr II 3866 Å line. The Cr II 4172 Å line is mixed in with the Fe-Ti 4172–9 Å blend, but the 4172 Å component is noticeably stronger.

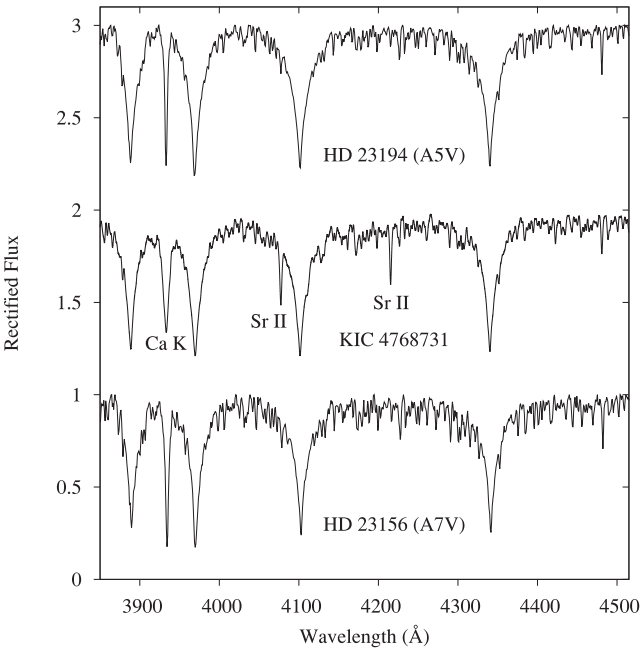

Figure 1. Spectrum of KIC 4768731 compared to the A5 V and A7 V MK standards. Note the prominent Sr II lines at 4077 Å and 4216 Å and the abnormal Ca II K line. The spectra have been offset for clarity.

Other features to look for in the spectrum of Ap stars include strong Eu and Si lines (for an atlas of Ap star spectra, see Gray & Corbally 2009). The Eu II 4205 Å line is enhanced, but the Eu II 4130 Å line is blended with the Si II doublet. That doublet of Si II (4128 and 4131 Å) is strong and, unlike in the comparison spectra, is more of a blended feature than a separated doublet. This is not a product of rotation, as KIC 4768731 is clearly not a rapid rotator, but could reflect a strong Eu line. The Si II 3856 Å line appears strong, but other Si II lines (4002, 4028 and 4076 Å) are not pronounced. These findings lead to the classification A5 Vp SrCr(Eu).

4 *Kepler* OBSERVATIONS

Debosscher et al. (2011) classified KIC 4768731 as exhibiting rotational modulation with a frequency of 0.191 206 d^{-1} (5.23 d) and an amplitude of 5.407 mmag. The AAVSO Variable Star Index (VSX; Watson, Henden & Price 2006) noted this star as ACV: (a suspected α^2 CVn variable) with a period of 5.21 d and magnitude range of 10 mmag based on *Kepler* light curves. The VSX entry by R. Jansen was dated 2011 May based on a phase plot of *Kepler* data from JD 245 4964 to 245 4998, noting also that the rise time from minimum to maximum light is 50 per cent of the variable's period.

One month of short-cadence (SC) data were acquired by KASC for this star in Q2.1 (2009 June 20–July 20), but with a 2-d gap due to a safe mode event. The star was, nevertheless, observed nearly continuously in long-cadence (LC) mode throughout the

[1] Spectra of the MK standards were obtained at R.O. Gray's website: http://stellar.phys.appstate.edu/Standards/std1_8.html

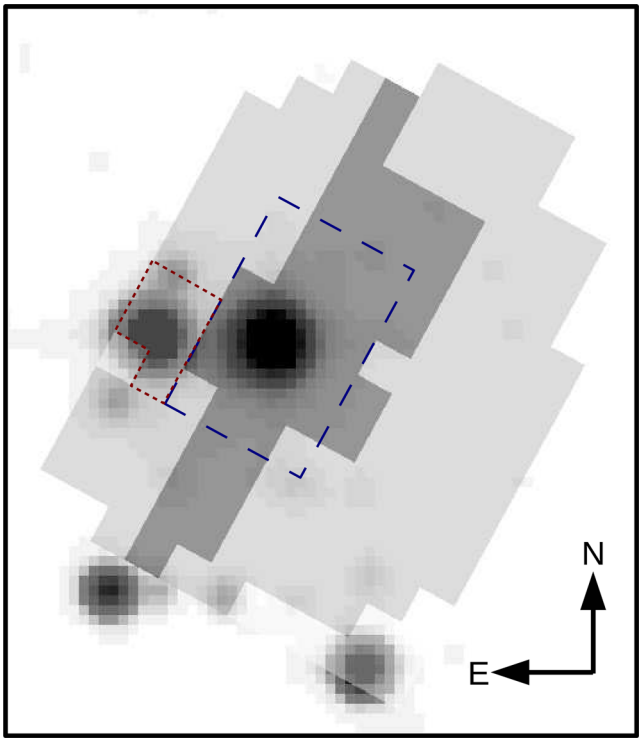

Figure 2. *Kepler* pixel map for the SC data overlaid on the 2MASS *J*-band image. The dark grey area contains the pixels used in the standard PDCSAP extraction and in light grey are all the pixels downloaded from the spacecraft. The areas highlighted in dashed and dotted lines are those used here to extract light curves of KIC 4768731 and KIC 4768748, respectively.

Kepler mission from Q0 to Q17 (2009 May 02–2013 May 2013). A periodogram of the SC data shows the previously reported rotational modulation, plus a weak higher frequency signal at 61.45 d^{-1}. The variability of KIC 4768731 obtained from the *Kepler* light curves is discussed in detail in Section 5.

The presence of the nearby companion star (KIC 4768748) could potentially affect the *Kepler* light curve of KIC 4768731. Fig. 2 shows the SC pixel map overlaid with the 2MASS *J*-band image. The standard PDCSAP light-curve extraction does not include the companion star, but it is very close. Therefore, using PYKE tools (Still & Barclay 2012), we extracted two light curves: one containing just the pixels centred on KIC 4768731 and the other centred on the companion star KIC 4768748. The light curve of KIC 4768748 contains neither the rotational modulation nor the high-frequency signal, while the light curve of KIC 4768731 show the previously reported rotational modulation plus the weak higher frequency signal.

5 FREQUENCY ANALYSIS OF THE *Kepler* DATA

KIC 4768731 was observed by *Kepler* in all quarters Q0–17 in LC, and during one month, Q2.1, in SC. We use these data to study the pulsation frequencies, amplitudes and phases for the full 4-yr data set. There is no Nyquist limitation with *Kepler* LC data, although there is a reduction in amplitude as a consequence of the pulsation periods being shorter than the integration times. See Murphy, Shibahashi & Kurtz (2013) for an explanation. Fig. 3 shows an amplitude spectrum of the Q0–17 data where only the low-frequency peaks generated by the rotational variation can be seen in the top panel. We ran a high-pass filter that removed the rotational

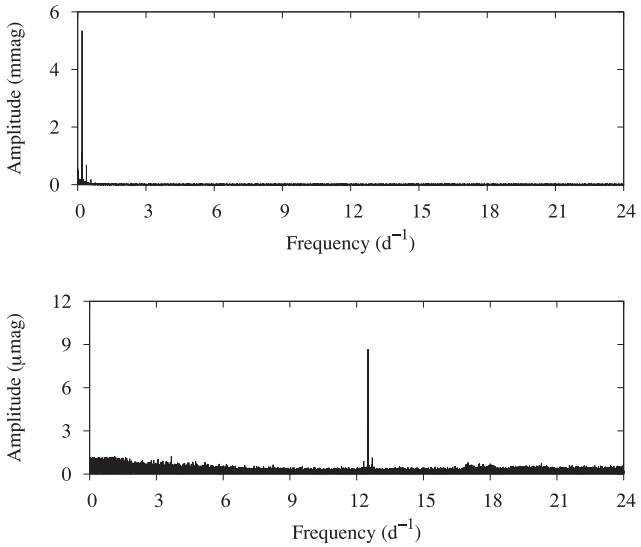

Figure 3. Top panel: an amplitude spectrum for the Q1 to Q17 *Kepler* LC data out to nearly the Nyquist frequency where only the low-frequency rotational variations can be seen, as a consequence of the scale. Bottom panel: an amplitude spectrum after a high-pass filter has removed the low-frequency variation showing the Nyquist alias of the 61.45-d^{-1} pulsation frequency triplet. Note the three orders of magnitude change in the ordinate scale from mmag in the top panel to μmag in the bottom panel.

variations from the light curves, and the lower panel of Fig. 3 shows the amplitude spectrum of those filtered data. There is a clear frequency triplet centred at 12.51 d^{-1}. A closer look at these peaks shows them to be Nyquist aliases of higher frequency peaks near 61.5 d^{-1}, as is evident from the SC data.

The rotation frequency found by fitting the highest peak in Fig. 3 to the LC data by non-linear least-squares gives $\nu_{\rm rot} = 0.191\,9622 \pm 0.000\,0003\,{\rm d}^{-1}$, or $P_{\rm rot} = 5.209\,358 \pm 0.000\,009$ d.

Fig. 4 shows an amplitude spectrum of the *Kepler* Q2.1 SC data in the top-left panel, where a clear peak is seen at 61.45 d^{-1}. After pre-whitening by the highest peak, the rotational sidelobes at $\nu_1 - \nu_{\rm rot}$ and $\nu_1 + \nu_{\rm rot}$ become evident on the lower-left panel. This frequency triplet is equally spaced and is evidence of an oblique dipole pulsation mode. This shows that the 12.51 d^{-1} peak seen in Fig. 3 is a Nyquist alias of this peak, since $61.45 - \nu_{\rm LC} = 12.51$, where $\nu_{\rm LC} = 48.94$ is the *Kepler* LC sampling frequency. The top-right panel of Fig. 4 therefore shows the same section of the amplitude spectrum for the entire Q0–17 *Kepler* LC data set, where the frequency resolution is the highest available. Of course, the amplitude is reduced because the integration times of the LC data are longer than the pulsation period. From Murphy (2012) we calculate the reduction factor to be $A/A_0 = \sin(\pi/n)/(\pi/n) = 5.5$, where n is the number of data points per oscillation cycle; this explains the lower amplitude in the LC data when compared to the SC data. The bottom-right panel then shows the amplitude spectrum of the LC data after pre-whitening by ν_1, where the rotational sidelobes can be seen, along with residual amplitude around ν_1. This residual amplitude is a consequence of frequency variability over the 4-yr data set, as we show below.

This triplet seen in Fig. 4 for both the SC and LC data is equally split by exactly the rotation frequency to better than 1σ. This is the signature of an oblique dipole pulsation mode. The three frequencies have been fitted to the data by a combination of linear and non-linear least-squares. Table 2 shows the results where the

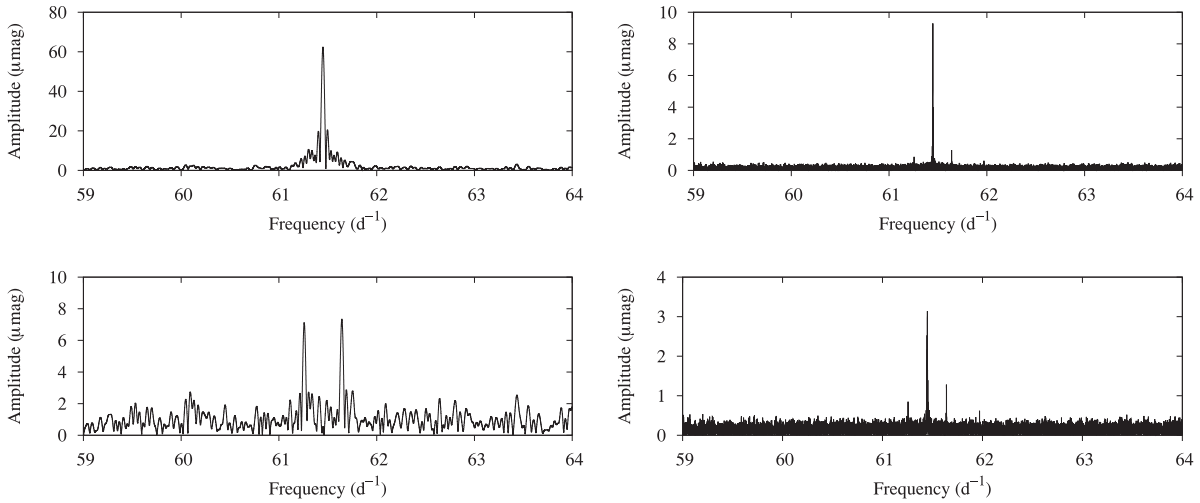

Figure 4. Top-left panel: an amplitude spectrum for the Q2.1 SC showing the pulsation frequency near 61.45 d^{-1}. Bottom-left panel: the SC data after pre-whitening by ν_1, where the rotational sidelobes are evident. Top-right panel: the same frequency range for the Q0–17 LC data where the oblique dipole pulsation triplet can be seen. Bottom-right panel: the LC data after pre-whitening by ν_1, where the rotational sidelobes are evident. The residual amplitude around ν_1 is the result of frequency or phase variability of the pulsation frequency over the 4-yr time span of the data set, as is seen in Fig. 5.

Table 2. A least-squares fit of the rotation frequency and the pulsational dipole triplet for KIC 4768731 to the full 4-yr *Kepler* LC data set. The zero-point of the time-scale is BJD2455697.97056, which coincides with pulsation amplitude maximum and rotational light maximum. This is typical for an oblique pulsator.

Labels	Frequency (d^{-1})	Amplitude (μmag)	Phase (rad)
	Rotation		
$\nu_{\rm rot}$	$0.191\,9622 \pm 0.000\,0003$	5368.3 ± 3.8	-3.0211 ± 0.0007
	Pulsation – long cadence (LC) data		
$\nu_1 - \nu_{\rm rot}$	$61.255\,837 \pm 0.000\,088$	0.8 ± 0.2	1.112 ± 0.222
ν_1	$61.447\,800 \pm 0.000\,008$	9.3 ± 0.2	1.117 ± 0.020
$\nu_1 + \nu_{\rm rot}$	$61.639\,762 \pm 0.000\,054$	1.3 ± 0.2	1.112 ± 0.147
	Pulsation – short cadence (SC) data		
$\nu_1 - \nu_{\rm rot}$	$61.255\,837 \pm 0.000\,088$	6.5 ± 0.7	2.842 ± 0.115
ν_1	$61.447\,800 \pm 0.000\,008$	62.2 ± 0.7	3.057 ± 0.012
$\nu_1 + \nu_{\rm rot}$	$61.639\,762 \pm 0.000\,054$	8.0 ± 0.7	2.842 ± 0.092

frequency splitting has been set to be exactly the rotation frequency. A time zero-point was selected to set the phases of the sidelobes equal, and we found that the phase of the central frequency is also equal, showing that the triplet is the result of pure amplitude modulation. This is typical of pure oblique dipole pulsation. We then find that the time of pulsation maximum, when all three frequencies of the triplet have the same phase, $t_0 = 245,\ 5697.970\,56$, coincides with maximum brightness of the rotational light modulation. That is shown by the phase of the rotational frequency, near $-\pi$, with that time zero-point. Because we have fitted a cosine function, and the data are in magnitudes, the phase at maximum rotational brightness is π rad. This can also be seen in the light curve, which we do not show here.

Maximum pulsation amplitude at rotational light minimum is expected for dipole oblique pulsation where the spots that produce the rotational light variations are aligned with the magnetic and pulsation poles. For KIC 4768731, the relationship differs by π rad from this simplest case, suggesting that the spots, magnetic field pole and pulsation pole lie in the same plane, but are not completely aligned. This is consistent with the improved oblique pulsator model (Bigot & Kurtz 2011).

We can constrain the pulsation geometry within the oblique pulsator model (Kurtz 1982; Bigot & Kurtz 2011) with the amplitudes of the components of the frequency triplet:

$$\tan i \tan \beta = (A_{+1} + A_{-1})/A_0,$$

where i is the rotational inclination, β is the inclination of the magnetic pole to the rotation axis, A_{+1}, A_{-1} and A_0 are the amplitudes of the rotational sidelobes and central frequency. From this equation, we obtain $\tan i \tan \beta = 0.226 \pm 0.031$ and $\tan i \tan \beta = 0.233 \pm 0.016$ from LC and SC data, respectively. Using the stellar radius and $v \sin i$ obtained from spectral analysis (Section 7) and the rotation period, we obtain values of $i = 40^{+24}_{-10}{}^{\circ}$ and $\beta = 15^{+9}_{-10}{}^{\circ}$. The angle between the magnetic and rotation axes is therefore relatively small. In addition, $i + \beta < 90^{\circ}$ and only one pole is seen, hence the simple, almost sinusoidal rotational light variations.

To study the residual amplitude around ν_1 seen for the LC data, we fitted ν_1 to 20-d sections of the data by least-squares and examined the time series of amplitude and phase. Fig. 5 shows that the amplitude is stable over the 4-yr time span, and the phase is variable. Since phase and frequency variability are indistinguishable, we interpret this as frequency variability. This is the source of

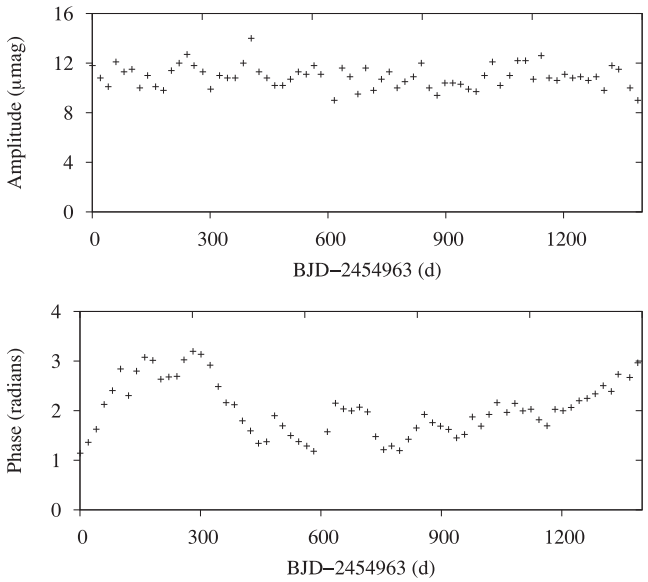

Figure 5. Top panel: pulsation amplitude of $\nu_1 = 61.4478\,\mathrm{d}^{-1}$ as a function of time for 20-d segments of the Q0–17 KIC 4768731 data. The amplitude is stable, but may have a secular decrease over the 4 yr. Bottom panel: pulsation phase for the same segments. There is clear variability in the pulsation phase. There is an apparent oscillation with a period of about half the *Kepler* orbital period, i.e. 186 d, which may be instrumental in origin. The larger, longer-term variations are most probably astrophysical in origin.

the residual amplitude in the amplitude spectrum that is unresolved from ν_1 as seen in the bottom-right panel of Fig. 4. Such frequency variability is known in many other roAp stars, as is discussed by Holdsworth et al. (2014b) for the roAp star KIC 7582608. The cause of such frequency variability is not yet known.

6 SPECTROSCOPIC OBSERVATIONS

To examine the abundances in detail and to investigate line profile variations as the star rotates, we obtained 33 high-resolution spectra.

Two high-resolution (R = 85 000) spectra covering the wavelength range 3780–9000 Å were obtained using the fibre-fed HERMES (Raskin et al. 2011) mounted on the 1.2-m Mercator Telescope at the Roque de los Muchachos Observatory, La Palma. The data were reduced using the HERMES DRS[2] pipeline software.

A further two high-resolution spectra with a resolution $R = 67\,000$ covering the wavelength region 3660–7360 Å were obtained with the 2.5-m Nordic Optical Telescope using the FIbre-fed Echelle Spectrograph (FIES; Telting et al. 2014). These spectra were extracted with the bespoke data reduction package, FIESTOOL.[3]

A series of 26 high-resolution spectra were obtained in 2013 August using the coudé-échelle spectrograph attached to the 2.0-m telescope at the Thüringer Landessternwarte (TLS) Tautenburg, Germany. The spectrograph has a resolving power of R = 63 000 and exposures cover the wavelength range from 4720 to 7360 Å. The spectra were reduced using standard ESO MIDAS packages. All spectra were corrected in wavelength for individual instrumental shifts by using a large number of telluric O_2 lines.

Table 3 gives the dates of the observations, along with the rotational phase ($\phi_{\rm rot}$) at the time of the midpoint of the exposures and measured RV (see Section 7.2). The rotational phase is obtained from the fractional part of (BJD − 2455697.97056) × 0.191 9622, where phase zero is the time of maximum light.

A TLS spectrum of the companion star, KIC 4768748, obtained on 2014 June 6, revealed that the star is indeed a late-K giant. In addition, the RV of this star is -2.9 ± 0.1 km s^{-1}, compared to -12.2 ± 0.2 km s^{-1} for KIC 4768731 (See Section 7.2). Thus, we conclude that the two stars are not physically associated, KIC 4768748 is a background giant.

7 SPECTROSCOPIC ANALYSIS

A detailed spectroscopic analysis of the 2011 HERMES spectrum was presented in Niemczura et al. (2015) who identified KIC 4768731 as an Ap CrSrEu star. Table 4 summarizes the basic stellar parameters obtained for this star.

7.1 Magnetic field

The ratio of the strengths of the Fe II 6147.7 Å and 6149.2 Å lines can be used to estimate the mean magnetic field modulus $\langle H \rangle$ (Mathys & Lanz 1992). From the individual spectra we obtain a mean value for the relative intensification of the Fe II 6147.7 Å line with respect to the Fe II 6149.2 Å line, $\Delta W_\lambda / \overline{W}_\lambda$, of 0.08 ± 0.03, where $\Delta W_\lambda = W_\lambda(6147.7) - W_\lambda(6149.2)$. This yields a mean magnetic field modulus, $\langle H \rangle$, of 2.7 ± 0.8 kG using the empirical relationship given in Mathys & Lanz (1992). The error bar includes both the scatter in the observed values of $\Delta W_\lambda / \overline{W}_\lambda$ and the uncertainty in the calibration for $\langle H \rangle$. The individual values for $\Delta W_\lambda / \overline{W}_\lambda$ show no significant variation with rotational phase.

For the magnetic modulus obtained above the splitting of the 6149.2 Å Zeeman doublet components would be ∼0.13 Å (Mathys et al. 1997). However, there is no sign of any splitting in our spectra due to the relatively large $v \sin i$ of this star.

7.2 RV variations?

A RV for each spectrum was determined by cross-correlation with a synthetic spectrum covering the wavelength range 5000–5800 Å using the parameters and abundances obtained from the detailed spectroscopic analysis. The barycentric RV are given in Table 3 and the formal uncertainties are 0.2 km s^{-1}. The average RV from the spectra obtained in 2013 is -12.2 ± 0.2 km s^{-1}. However, Fehrenbach & Burnage (1990) reported a value of -29 ± 1.2 km s^{-1} based on four observations obtained on 1984 June 27, 1986 August 2, 30 and 31. They used the Fehrenbach Objective Prisms on the Schmidt telescope at the Observatorie de Haute-Provence and the external error is given as 3.5 km s^{-1}. The difference between the two epochs of ∼17 km s^{-1} suggests that the star could be a spectroscopic binary. The HERMES spectrum taken in 2011 July has an RV that is consistent with those taken during 2013 August. In 2014 June and 2015 May, we obtained further TLS spectra and their RV values are consistent with the previous years (Fig. 6). Hence, we find no significant change in RV over a period of 4 yr.

7.3 Spectral line profile variations

The individual spectra were examined for evidence of spectral line profile variations with rotational phase. The Hα and Hβ Balmer lines and the Na D lines do not show any variation with phase. Similarly, the HERMES and FIES spectra of the Ca H&K lines do not show any variation with rotational phase, but have the unusual

[2] http://www.mercator.iac.es/instruments/hermes/hermesdrs.php
[3] http://www.not.iac.es/instruments/fies/fiestool/

Table 3. Log of spectral observations of KIC 4768731. Date and BJD are given for the mid-point of the exposure.

Instrument	Date	Exp time (s)	S/N	BJD (TDB)	$\phi_{\rm rot}$	RV (km s^{-1})
HERMES	2011 Jul 13 22:53:56	1900	87	2455756.45765	0.227	−12.0
FIES	2013 Aug 04 00:43:06	2000	102	2456508.53370	0.597	−12.3
FIES	2013 Aug 06 00:19:54	1748	112	2456510.51759	0.978	−11.8
HERMES	2013 Aug 10 03:26:10	1800	80	2456514.64693	0.771	−12.2
TLS	2013 Aug 14 22:59:41	1800	80	2456519.46185	0.695	−12.3
TLS	2013 Aug 14 23:30:42	1800	73	2456519.48339	0.699	−12.3
TLS	2013 Aug 15 00:01:43	1800	70	2456519.50493	0.703	−12.4
TLS	2013 Aug 15 00:32:44	1800	63	2456519.52646	0.708	−12.4
TLS	2013 Aug 15 01:41:49	1800	58	2456519.57444	0.717	−12.3
TLS	2013 Aug 15 02:12:50	1800	49	2456519.59598	0.721	−12.3
TLS	2013 Aug 15 02:43:51	1800	46	2456519.61752	0.725	−11.7
TLS	2013 Aug 15 21:54:18	2400	108	2456520.41643	0.879	−12.1
TLS	2013 Aug 16 01:58:32	2400	85	2456520.58604	0.911	−12.7
TLS	2013 Aug 16 21:44:06	2400	95	2456521.40934	0.069	−12.4
TLS	2013 Aug 17 01:59:27	2400	71	2456521.58667	0.103	−12.4
TLS	2013 Aug 17 22:59:50	2400	89	2456522.46192	0.271	−12.3
TLS	2013 Aug 21 19:54:11	2400	76	2456526.33295	0.014	−11.9
TLS	2013 Aug 22 20:10:07	2400	72	2456527.34400	0.208	−11.9
TLS	2013 Aug 23 19:51:48	2400	76	2456528.33127	0.398	−12.2
TLS	2013 Aug 24 00:50:49	2417	70	2456528.53891	0.438	−12.2
TLS	2013 Aug 26 20:58:21	2400	67	2456531.37743	0.983	−12.4
TLS	2013 Aug 26 22:25:29	2400	78	2456531.43794	0.994	−12.4
TLS	2013 Aug 26 23:06:30	2400	73	2456531.46642	1.000	−12.3
TLS	2013 Aug 27 01:42:35	2400	60	2456531.57481	0.021	−12.3
TLS	2013 Aug 27 20:42:41	2400	45	2456532.36653	0.172	−12.1
TLS	2013 Aug 27 21:24:35	2400	98	2456532.39563	0.178	−12.2
TLS	2013 Aug 27 22:07:30	2400	95	2456532.42543	0.184	−12.3
TLS	2013 Aug 27 22:48:31	2400	84	2456532.45392	0.189	−12.3
TLS	2013 Aug 27 23:29:32	2400	90	2456532.48240	0.195	−12.4
TLS	2013 Aug 28 00:10:33	2400	76	2456532.51088	0.200	−12.3
TLS	2014 Jun 17 23:10:15	2400	86	2456826.46545	0.628	−12.4
TLS	2015 May 10 22:55:57	2400	84	2457153.45487	0.398	−12.2
TLS	2015 May 11 01:07:39	2400	75	2457153.54733	0.416	−12.1

Notes: The rotational phase ($\phi_{\rm rot}$) is given by the fractional part of (BJD − 2455697.97056) × 0.191 9622, where phase zero is the time of maximum light. The signal-to-noise ratio (S/N) obtained using the DER_SNR algorithm (Stoehr et al. 2008).

Table 4. Basic stellar parameters of KIC 4768731.

Parameter	Value	Units
$T_{\rm eff}$	8100 ± 200	K
log g	4.0 ± 0.2	
[Fe/H]	+0.31 ± 0.24	
$V_{\rm micro}$	0.5 ± 0.3	km s^{-1}
$v \sin i$	14.8 ± 1.6	km s^{-1}
M	2.11 ± 0.27	M$_\odot$
R	2.39 ± 0.68	R$_\odot$
log L	1.34 ± 0.25	L$_\odot$
M_V	1.43 ± 0.67	mag.
Sp. type	A5 Vp SrCr(Eu)	

Note: Mass (M) and radius (R) are estimated using the Torres, Andersen & Giménez (2010) calibration.

line profiles associated with abundance stratification in the atmosphere (Babel 1994; Ryabchikova et al. 2002). The sharp cores of Ca H&K lines can be recreated using a step-shaped stratified abundance profile with [Ca/H] = +1.0 dex for layers deeper than log (τ_{5000}) = −1.0 and [Ca/H] = −2 dex for higher layers (Fig. 7). In contrast, a global enhancement of [Ca/H] = +0.5 dex is unable to reproduce the observed line profile.

The HERMES and FIES spectra of the Sr II 4077.7 Å line shows considerable variation with rotational phase (Fig. 8). The line is strongest at $\phi_{\rm rot}$ = 0.978 and weakest at $\phi_{\rm rot}$ = 0.597. This is consistent with the weakest line strength occurring at or around $\phi_{\rm rot}$ = 0.5. The other two spectra are very similar, but their phases with respect to $\phi_{\rm rot}$ = 0.5 are −0.271 and +0.273, respectively. This suggests that there is a region of enhanced Sr crossing the stellar meridian at the time of maximum light ($\phi_{\rm rot}$ = 0.0).

Fig. 9 shows the variation of the Y II 4883.7 Å line profile with rotational phase. There is a clear absorption feature moving redwards with increasing phase, first appearing on the blue edge of the line profile at around $\phi_{\rm rot}$ = 0.1 and disappearing around $\phi_{\rm rot}$ = 0.9. The feature crosses the centre of the line around $\phi_{\rm rot}$ = 0.5, coinciding with the time of minimum light in the rotation cycle. Similar behaviour is seen in the Y II 4900.1 and Ba II 6141.7 Å lines. This is in antiphase to the variation of the Sr II line.

Fig. 10 shows the variation of the Eu II 6437.6 Å line profile with rotational phase. The line is quite weak around $\phi_{\rm rot}$ = 0.4. By $\phi_{\rm rot}$ = 0.7 an absorption feature can be seen in the blue wing of the profile. As phase increases the feature moves redwards across the line profile, reaching a maximum around $\phi_{\rm rot}$ = 0.0 when it is

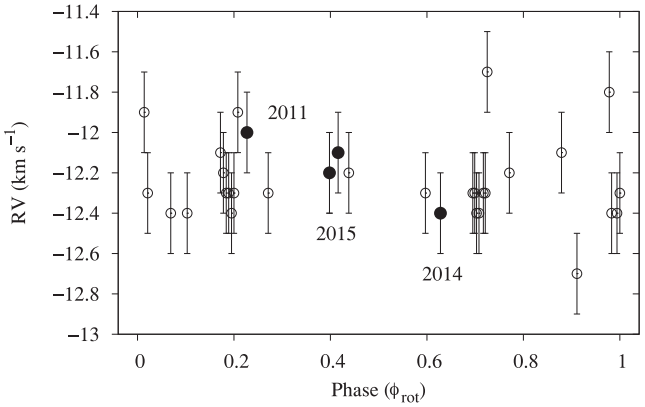

Figure 6. RV measurements show no trend with rotational phase. The filled circles indicate the values obtained in 2011, 2014and 2015 and show that they are not significantly different from those from 2013 (open circles).

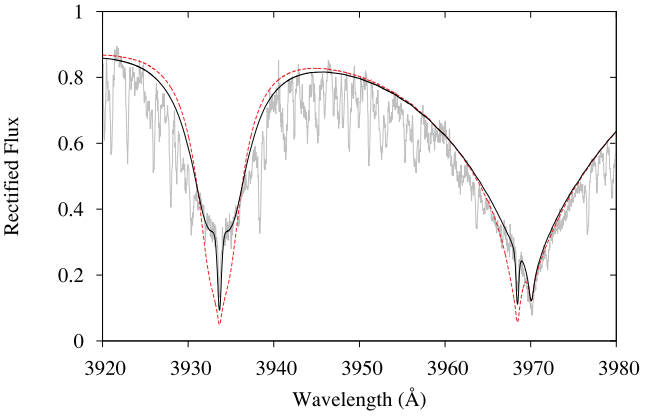

Figure 7. The Ca H&K lines in the FIES spectrum (grey line) taken on 2013 August 6 shows the distinctive pointed core due to element stratification. The solid line shows a synthetic line profile created using a step-shaped stratified abundance profile, while the red dashed line shows a normal non-stratified synthesis.

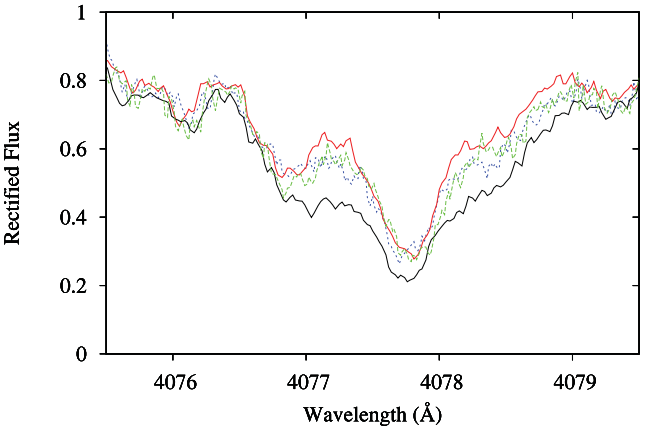

Figure 8. Variations in the profile shape of the Sr II 4077.7 Å line with rotational modulation phase. The solid black line was taken at $\phi_{rot} = 0.978$, the solid red line at $\phi_{rot} = 0.597$. The dashed green and dotted blue lines were taken at $\phi = 0.771$ and $\phi_{rot} = 0.227$, respectively.

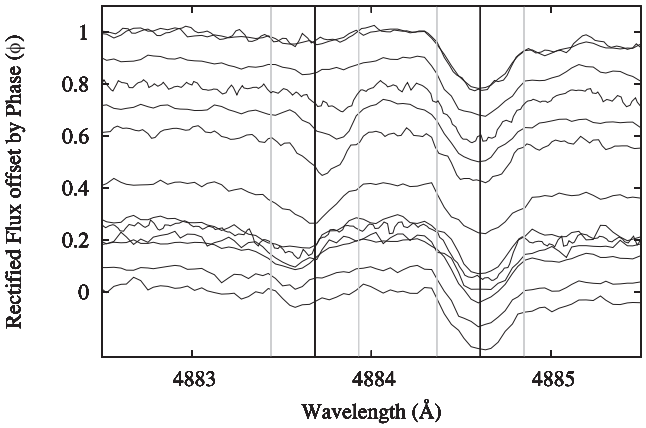

Figure 9. Changes in line profile strength and shape with rotational phase for the Y II line at 4883.7 Å. The rectified spectra have been offset so that their continuum levels correspond to their rotational phases. The nearby Cr II line at 4884.6 Å shows little shape variation with phase. The vertical black and grey lines indicate the line centres and the ±15 km s^{-1} $v \sin i$ widths, respectively.

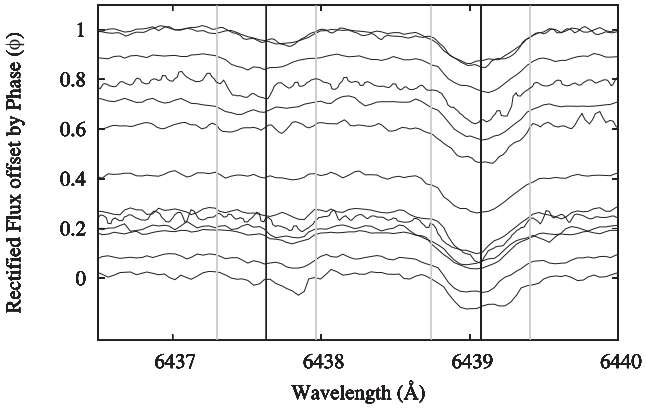

Figure 10. Changes in line profile strength and shape with rotational phase for the Eu II line at 6437.6 Å. The rectified spectra have been offset so that their continuum levels correspond to their rotational phases. The nearby Ca I line at 6439.1 Å shows little shape variation with phase. The vertical black and grey lines indicate the line centres and the ±15 km s^{-1} $v \sin i$ widths, respectively.

close to the line centre. The feature then moves to the red wing and weakens, disappearing around $\phi_{rot} = 0.2$. Similar behaviour is seen in other Eu lines. The variations in the Eu lines are in antiphase with those for Y and Ba lines, but in phase with the Sr line.

To further investigate line strength variations with rotational phase, we selected six nights in 2013 August with multiple TLS spectra. For each night the spectra were co-added to produce a single nightly spectrum with signal-to-noise ratios (S/N) in the range 100–150. For each of the six spectra abundances were obtained using the same spectral synthesis methodology as Niemczura et al. (2015). The results of the spectral fitting are given in Table 5. The overall abundance pattern is consistent with that found by Niemczura et al. (2015) and with the spectral classification presented in Section 3: Cr is considerably enhanced, Eu is modestly enhanced, while Ca and Si are relatively normal. V and Co are also considerably enhanced and there is general modest (∼+0.3 dex) overabundance of most other transition-group elements, with the exception of Sc, which is depleted by over 0.5 dex. Several elements, Mg, Si, Cr, Co and Eu, have abundance variations in phase with rotation – they are strongest

Table 5. Elemental abundances obtained for KIC 4768731 from TLS spectra. Abundances are given in the form $\log A(\mathrm{El}) = \log(N_{\mathrm{El}}/N_{\mathrm{H}}) + 12$ obtained from spectra taken on six different nights and rotational phases (ϕ_{rot}). n is the maximum number of lines for an element used in the abundance averages, which can be slightly fewer at different rotational phases. Line-to-line standard deviation error bars are given when $n > 2$. In column 9, the solar abundances from Asplund et al. (2009) are given in for reference.

El	n	Aug 14–15 ($\phi_{\mathrm{rot}} = 0.71$)	Aug 15–16 ($\phi_{\mathrm{rot}} = 0.89$)	Aug 16–17 ($\phi_{\mathrm{rot}} = 0.09$)	Aug 23–24 ($\phi_{\mathrm{rot}} = 0.42$)	Aug 26–27 ($\phi_{\mathrm{rot}} = 1.00$)	Aug 27–28 ($\phi_{\mathrm{rot}} = 0.19$)	Solar
C	19	8.45 ± 0.33	8.26 ± 0.27	8.47 ± 0.36	8.51 ± 0.28	8.43 ± 0.34	8.46 ± 0.37	8.43
N	1	8.16	8.38	8.06	8.20	7.94	8.15	7.83
O	5	9.37 ± 0.22	9.10 ± 0.51	9.14 ± 0.41	8.62 ± 0.55	9.16 ± 0.42	9.40 ± 0.21	8.69
Na	3	7.13 ± 0.06	7.08	7.21 ± 0.12	6.81 ± 0.31	7.22 ± 0.12	6.77	6.24
Mg	8	7.83 ± 0.18	7.87 ± 0.21	7.82 ± 0.20	7.73 ± 0.17	7.86 ± 0.20	7.84 ± 0.16	7.60
Al	2	7.47	7.43	7.45	7.04	7.34	7.15	6.45
Si	34	7.53 ± 0.27	7.66 ± 0.24	7.75 ± 0.21	7.45 ± 0.26	7.74 ± 0.23	7.56 ± 0.22	7.51
S	9	7.34 ± 0.43	7.56 ± 0.49	7.57 ± 0.25	7.02 ± 0.26	7.27 ± 0.33	7.22 ± 0.34	7.12
Ca	18	6.81 ± 0.21	6.77 ± 0.20	6.88 ± 0.21	6.80 ± 0.18	6.81 ± 0.20	6.83 ± 0.22	6.34
Sc	7	2.45 ± 0.10	2.47 ± 0.35	2.46 ± 0.33	2.66 ± 0.45	2.30 ± 0.35	2.53 ± 0.45	3.15
Ti	42	5.08 ± 0.29	5.00 ± 0.28	5.13 ± 0.25	5.12 ± 0.24	5.17 ± 0.24	5.19 ± 0.27	4.95
V	8	5.10 ± 0.30	5.17 ± 0.30	5.19 ± 0.28	5.14 ± 0.30	5.22 ± 0.28	5.21 ± 0.24	3.93
Cr	111	7.36 ± 0.18	7.50 ± 0.18	7.51 ± 0.17	7.21 ± 0.16	7.55 ± 0.17	7.38 ± 0.19	5.64
Mn	17	5.77 ± 0.35	5.82 ± 0.36	5.72 ± 0.32	5.79 ± 0.28	5.84 ± 0.34	5.69 ± 0.30	5.43
Fe	142	7.79 ± 0.18	7.83 ± 0.18	7.83 ± 0.17	7.80 ± 0.19	7.81 ± 0.18	7.83 ± 0.18	7.50
Co	6	5.78 ± 0.25	6.11 ± 0.37	6.14 ± 0.33	5.84 ± 0.24	6.28 ± 0.26	5.74 ± 0.18	4.99
Ni	31	6.30 ± 0.34	6.37 ± 0.36	6.33 ± 0.37	6.18 ± 0.28	6.24 ± 0.35	6.39 ± 0.31	6.22
Cu	1	3.09	3.05	3.12	3.34	3.63	3.08	4.19
Zn	1	4.73	4.70	4.53	4.68	4.69	4.72	4.56
Y	9	3.05 ± 0.24	2.74 ± 0.39	2.90 ± 0.25	3.12 ± 0.21	2.82 ± 0.20	2.79 ± 0.35	2.21
Zr	3	3.60	4.67 ± 0.77	4.36 ± 0.69	3.49	3.48	4.27 ± 0.58	2.58
Ba	2	2.50	1.81	1.87	2.52	1.80	2.05	2.18
La	2	1.60	1.34	1.91	0.77	1.23	1.75	1.10
Nd	6	2.34 ± 0.15	2.24 ± 0.02	2.31 ± 0.14	2.19 ± 0.24	2.40 ± 0.02	2.28 ± 0.06	1.42
Eu	3	2.65 ± 0.31	2.50 ± 0.11	2.33 ± 0.36	1.93 ± 0.50	2.47 ± 0.34	2.20 ± 0.26	0.52

when the star is the brightest. In addition, the same behaviour was noted for the Sr line above. The Y and Ba lines, on the other hand, vary in antiphase with rotation – they are strongest when the star is the faintest. Other elements, including Ca, Ti, V, Mn and Fe, show little variation with phase or the results are inconclusive.

To search for the presence of other rare earth elements, the individual TLS spectra from 2013 were co-added to produce a single spectrum with an S/N of 245. This spectrum was visually searched for lines due to various rare earth elements. With the exception of the already detected La, Nd and Eu, only tentative detections or upper limits were obtained (see Table 6).

The relatively large, and variable, scatter in the standard deviations of some of the abundances obtained is probably the result of the surface inhomogeneities and vertical stratification present in the atmosphere of this Ap star. A detailed spectral analysis taking into account surface inhomogeneities and abundance stratification will be presented in Niemczura et al. (in preparation).

Table 6. Rare earth elements in KIC 4768731. Abundances are given in the form $\log A(\mathrm{El}) = \log(N_{\mathrm{El}}/N_{\mathrm{H}}) + 12$. A colon (:) indicates a tentative detection, where other lines of the element have upper limits below the given value. n is the number of lines used to obtain the abundance averages, except in the cases of upper limits or tentative detections where it is the number of lines searched. In column 4, the solar abundances from Asplund et al. (2009) are given in for reference.

El	n	$\log A(\mathrm{El})$	Solar
La	2	1.40	1.10
Ce	6	<2.5	1.58
Pr	3	3.2:	0.72
Nd	6	2.25 ± 0.12	1.42
Sm	2	2.2:	0.96
Eu	3	2.45 ± 0.11	0.52
Gd	4	3.0:	1.07
Tb	3	<2.5	0.30
Dy	4	<3.3	1.10
Er	2	3.5:	0.92
Tm	2	<2.5	0.10
Yb	6	<3.5	0.84
Lu	5	<2.0	0.10

8 NON-ADIABATIC OSCILLATION MODELLING

The mechanism responsible for exciting the oscillations observed in roAp stars is still not fully understood. The opacity mechanism acting on the hydrogen ionization region leads to the excitation of high radial-order acoustic pulsations in models of cool Ap stars with fully radiative envelopes, where convection is assumed to be suppressed by the strong magnetic field (Balmforth et al. 2001). This mechanism has been shown to provide a promising explanation for the observed pulsations in roAp stars with pulsation frequencies below the acoustic cut-off (Cunha 2002). However, in a fraction of the known roAp pulsators, the observed frequencies are too high to be driven in this way (Cunha et al. 2013) and an alternative mechanism needs to be considered, such as the effect of turbulent

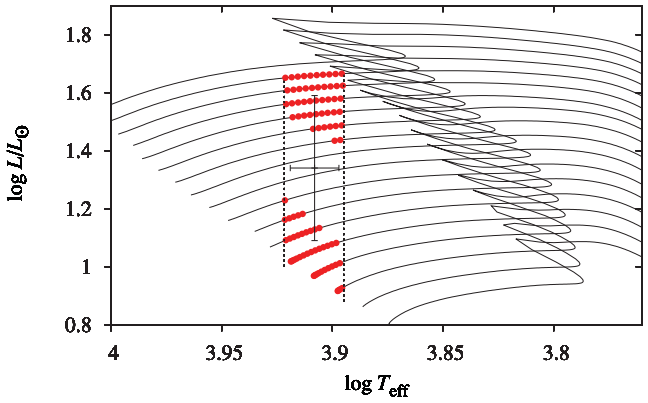

Figure 11. HR diagram showing the results of the non-adiabatic oscillation modelling. The cross indicates the location and 1σ uncertainty of KIC 4768731. The solid lines are the evolutionary tracks (starting from the ZAMS) covering masses from 1.6 $M_\odot$ (bottom) to 2.4 (top) in steps of 0.05 $M_\odot$. The vertical dashed lines indicate the range in temperatures searched. Models found to be unstable at the observed frequency are marked by filled circles. In the lower luminosity region, the modes excited are of low radial-order, while in the higher luminosity region they are of high radial-order.

pressure suggested by Cunha et al. (2013) and recently found to be a likely explanation for pulsations in an Am star (Antoci et al. 2014).

The oscillation frequency observed in KIC 4768731 is below the acoustic cut-off frequency derived from models covering the region of the HR diagram where the star is located. To check if the opacity mechanism can drive the observed pulsation, and further constrain the global parameters of the star, we carried out a linear, non-adiabatic stability analysis of a grid of models covering that region of the HR diagram. Evolutionary tracks were produced with the MESA stellar evolution code (Paxton et al. 2013) for stellar masses in the range 1.6–2.4 $M_\odot$, in intervals of 0.05 $M_\odot$, and with initial mass fraction of hydrogen and helium of $X = 0.70$ and $Y = 0.28$, respectively. Mixing beyond the convective core during the main sequence has been considered, taking the convective overshoot parameter defined in Paxton et al. (2013, their equation 9) to be $f_{\rm ov} = 0.016$. Only models with $T_{\rm eff}$ in the range 7850–8350 K were considered for the stability analysis (vertical dashed lines in Fig. 11). The mass, luminosity and effective temperature extracted from the MESA models were used to generate the equilibrium models necessary for the non-adiabatic computations.

The non-adiabatic analysis followed closely that of Cunha et al. (2013), except that we have considered only their 'polar' models (models with fully radiative envelopes) as these are the models in which roAp-type pulsations are found to be driven by the opacity mechanism. Following that work, for each set of mass, luminosity and effective temperature, we have considered four different case studies. In the first (or *standard*) case the equilibrium model has a surface helium abundance of $Y_{\rm sur} = 0.01$ and an atmosphere that extends to a minimum optical depth of $\tau_{\rm min} = 3.5 \times 10^{-5}$. Moreover, in the pulsation analysis a fully reflective boundary condition is applied at the surface for this case study. The other three case studies are obtained by swapping these properties, one at the time to: $Y_{\rm sur} = 0.1$, $\tau_{\rm min} = 3.5 \times 10^{-4}$ and a transmissive boundary condition. Together, these four case studies cover the main uncertainties in the modelling. If modes with frequencies similar to that observed in KIC 4768731 are found unstable in at least one of the case studies, then the corresponding model parameter set is identified as unstable at the observed frequency.

Models found to be unstable at the observed frequency are marked by filled circles in Fig. 11. Inspection of this figure shows that there are two independent regions within the part of the HR diagram explored in which pulsations with the observed frequency are predicted to be excited. In the lower luminosity region, the modes excited at the observed frequency are of low radial-order, characteristic of δ-Scuti stars, while in the higher luminosity region they are of high radial-order, characteristic of roAp stars.

The non-adiabatic analysis performed here does not include the direct effect of the magnetic field on pulsations, but only its indirect effect through the suppression of convection in the stellar envelope. However, it is known from studies addressing the direct effect of the magnetic field that the coupling of acoustic and magnetic waves in the outer layers of roAp stars leads to wave energy losses through the dissipation of acoustic waves in the atmosphere (Sousa & Cunha 2008) and magnetic waves in the interior (Cunha & Gough 2000). In fact, Saio (2005) has shown that energy losses through the latter process are particularly significant for low radial-order modes. These modes are then stabilized, explaining their absence in roAp stars. If this is the case for KIC 4768731, then the lower luminosity unstable region shown in Fig. 11 is likely to be spurious, resulting from the non-inclusion of the direct effect of the magnetic field on pulsations in the non-adiabatic computations. Our non-adiabatic calculations thus point to KIC 4768731 being a relatively evolved and luminous star.

9 DISCUSSION AND CONCLUSIONS

Given the identification of KIC 4768731 as an Ap star, the pulsation is almost certainly of the roAp type and with a frequency of 61.45 d^{-1} (corresponding to a period of 23.43 min), this star only just misses out on being the longest period roAp star known (HD 177765; Alentiev et al. 2012, 23.56 min). Other low-frequency roAp stars, discovered from their low-amplitude RV variations, include HD 116114 (21 min) and β CrB (16.2 min) (Elkin et al. 2005a; Kurtz, Elkin & Mathys 2007a). All four of these stars occupy a similar location in the HR diagram, around $T_{\rm eff} = 8000$ K and $\log g = 4.0$, with KIC 4768731 having the shortest rotation period.

Spectral lines from rare earth elements are usually strong in Ap stars (Wolff 1983). However, we find a distinct lack of significant overabundances in rare earth elements compared to those found in other roAp stars of similar effective temperatures: HD 177765 (Alentiev et al. 2012), HD 116114 and β CrB (Ryabchikova et al. 2004) (Fig. 12). A similar conclusion was found for another, cooler, *Kepler* roAp star, KIC 10195926 (Elkin et al. 2014).

The Mg, Si, Cr, Co, Sr and Eu lines in KIC 4768631 show line strength variations in phase with rotation – they are strongest when the star is the brightest. The Y and Ba lines, on the other hand, vary in antiphase with rotation – they are strongest when the star is the faintest. Other elements, including Ca and Fe, show little variation with rotational phase or the results are inconclusive. The pulsation analysis has shown that the pulsation axis is in the same plane as the abundance spots that lead to rotational light maximum, but not completely aligned. The pulsations are coincident with light maximum, hence with Sr II maximum, and out of phase with Y II maximum. Where the pulsation axis, magnetic poles and spots are located is problematic, but they appear to lie in a single plane, which is consistent with the improved oblique pulsator model of Bigot & Kurtz (2011). KIC 4768631, however, is unusual in having

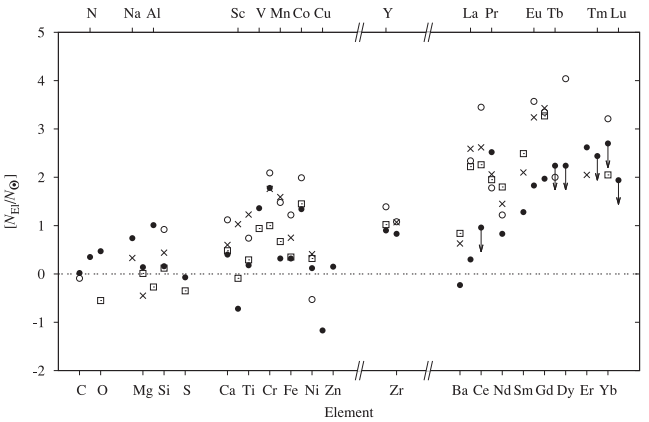

Figure 12. Abundance patterns for KIC 4768731 (filled circles), HD 177765 (open circles), HD 116114 (open squares) and β CrB (crosses). Upper limits are indicated by downward pointing arrows. Abundances are given relative to the solar values from Asplund et al. (2009).

pulsation maximum at maximum rotational brightness. Many roAp stars have pulsation maximum at rotational light minimum, which can be associated with strong rare earth element spots.

It tends to be the slow rotators, with periods longer than one month, that have aligned rotation and magnetic axes (Landstreet & Mathys 2000), or the more evolved stars, since North (1985) found essentially random angles of alignment for near-ZAMS stars (for a review, see Murphy 2014). The former is ruled out by the 5.2 d rotation period, but the latter case is a possibility since the non-adiabatic modelling suggests that the roAp-type pulsations would be expected for the star nearer the terminal-age main sequence than the ZAMS. The luminosity, and hence age, of KIC 4768731 is, however, uncertain due to the lack of an independent distance determination. Furthermore, Ap (SrCrEu) stars are supposed to take about half their main-sequence lifetime to develop their peculiarities (Abt 2009), so the age is of interest. If Abt is right, then perhaps this star is not old enough to have accumulated very anomalous rare earth elements. Hence, KIC 4768731 may prove to be an interesting test case for the development of chemical peculiarities in Ap stars.

ACKNOWLEDGEMENTS

This work made use of PYKE (Still & Barclay 2012), a software package for the reduction and analysis of *Kepler* data. This open source software project is developed and distributed by the NASA Kepler Guest Observer Office.

Part of this work is based on observations obtained with the HERMES spectrograph, which is supported by the Fund for Scientific Research of Flanders (FWO), Belgium, the Research Council of K.U. Leuven, Belgium, the Fonds National de la Recherche Scientifique (F.R.S.-FNRS), Belgium, the Royal Observatory of Belgium, the Observatoire de Genée, Switzerland, and the TLS, Germany.

Calculations have been carried out in Wrocław Centre for Networking and Supercomputing (http://www.wcss.pl), grant no. 214.

EN acknowledges support from the NCN grant no. 2014/13/B/ST9/00902. SJM acknowledges research support by the Australian Research Council. Funding for the Stellar Astrophysics Centre is provided by the Danish National Research Foundation (grant agreement no.: DNRF106). The research is supported by the ASTERISK project (ASTERoseismic Investigations with SONG and Kepler) funded by the European Research Council (grant agreement no.: 267864). MSC is supported by FCT through research grant UID/FIS/04434/2013 and through the Investigador FCT contract of reference IF/00894/2012 and POPH/FSE (EC) by FEDER funding through the programme COMPETE. Funds for this work were provided also by the EC, under FP7, through the project FP7-SPACE-2012-31284. LAB wishes to thank the National Research Foundation of South Africa for financial support. MB is F.R.S.-FNRS Postdoctoral Researcher, Belgium. AOT acknowledges support from Sonderforschungsbereich SFB 881 'The Milky Way System' (subprojects A4 and A5) of the German Research Foundation (DFG).

REFERENCES

Abt H. A., 2009, AJ, 138, 28
Alentiev D., Kochukhov O., Ryabchikova T., Cunha M., Tsymbal V., Weiss W., 2012, MNRAS, 421, L82
Antoci V. et al., 2014, ApJ, 796, 118
Asplund M., Grevesse N., Sauval A. J., Scott P., 2009, ARA&A, 47, 481
Babcock H. W., 1947, ApJ, 105, 105
Babel J., 1994, A&A, 283, 189
Balmforth N. J., Cunha M. S., Dolez N., Gough D. O., Vauclair S., 2001, MNRAS, 323, 362
Balona L. A. et al., 2011a, MNRAS, 410, 517
Balona L. A. et al., 2011b, MNRAS, 413, 2651
Bigot L., Kurtz D. W., 2011, A&A, 536, A73
Bychkov V. D., Bychkova L. V., Madej J., 2009, MNRAS, 394, 1338
Cannon A. J., 1925, Ann. Harv. Coll. Obser., 100, 17
Cunha M. S., 2002, MNRAS, 333, 47
Cunha M. S., Gough D., 2000, MNRAS, 319, 1020
Cunha M. S., Alentiev D., Brandão I. M., Perraut K., 2013, MNRAS, 436, 1639
Debosscher J., Blomme J., Aerts C., De Ridder J., 2011, A&A, 529, A89
Donati J.-F., Landstreet J. D., 2009, ARA&A, 47, 333
Elkin V. G., Riley J. D., Cunha M. S., Kurtz D. W., Mathys G., 2005a, MNRAS, 358, 665
Elkin V. G., Kurtz D. W., Mathys G., Wade G. A., Romanyuk I. I., Kudryavtsev D. O., Smolkin S., 2005b, MNRAS, 358, 1100
Elkin V. G., Kurtz D. W., Mathys G., Freyhammer L. M., 2010, MNRAS, 404, L104
Elkin V. G., Kurtz D. W., Shibahashi H., Saio H., 2014, MNRAS, 444, 1344
Fehrenbach C., Burnage R., 1990, A&AS, 83, 91
Girish V. et al., 2001, A&A, 380, 142
González J. F., Hubrig S., Kurtz D. W., Elkin V., Savanov I., 2008, MNRAS, 384, 1140
Gray R. O., Corbally J. C., 2009, Stellar Spectral Classification. Princeton Univ. Press, Princeton, NJ
Gruberbauer M. et al., 2008, A&A, 480, 223
Handler G. et al., 2002, MNRAS, 330, 153
Handler G. et al., 2006, MNRAS, 366, 257
Holdsworth D. L., 2015, PhD thesis, Keele University, UK
Holdsworth D. L. et al., 2014a, MNRAS, 439, 2078
Holdsworth D. L., Smalley B., Kurtz D. W., Southworth J., Cunha M. S., Clubb K. I., 2014b, MNRAS, 443, 2049
Huber D. et al., 2008, A&A, 483, 239
Høg E. et al., 2000, A&A, 355, L27
Kochukhov O., Landstreet J. D., Ryabchikova T., Weiss W. W., Kupka F., 2002, MNRAS, 337, L1
Kochukhov O., Ryabchikova T., Bagnulo S., Lo Curto G., 2008a, Contrib. Astron. Obser. Skalnate Pleso, 38, 423
Kochukhov O., Ryabchikova T., Bagnulo S., Lo Curto G., 2008b, A&A, 479, L29
Kochukhov O., Bagnulo S., Lo Curto G., Ryabchikova T., 2009, A&A, 493, L45
Kochukhov O., Alentiev D., Ryabchikova T., Boyko S., Cunha M., Tsymbal V., Weiss W., 2013, MNRAS, 431, 2808

Kreidl T. J., Kurtz D. W., Bus S. J., Kuschnig R., Birch P. B., Candy M. P., Weiss W. W., 1991, MNRAS, 250, 477
Kurtz D. W., 1982, MNRAS, 200, 807
Kurtz D. W., Martinez P., 1994, Inf. Bull. Var. Stars, 4013, 1
Kurtz D. W., Martinez P., 1995, Inf. Bull. Var. Stars, 4209, 1
Kurtz D. W., Sullivan D. J., Martinez P., Tripe P., 1994a, MNRAS, 270, 674
Kurtz D. W., Martinez P., Tripe P., 1994b, MNRAS, 271, 421
Kurtz D. W., Martinez P., Koen C., Sullivan D. J., 1996, MNRAS, 281, 883
Kurtz D. W., van Wyk F., Roberts G., Marang F., Handler G., Medupe R., Kilkenny D., 1997a, MNRAS, 287, 69
Kurtz D. W., Martinez P., Tripe P., Hanbury A. G., 1997b, MNRAS, 289, 645
Kurtz D. W. et al., 2002, MNRAS, 330, L57
Kurtz D. W., Elkin V. G., Mathys G., 2005, MNRAS, 358, L6
Kurtz D. W., Elkin V. G., Cunha M. S., Mathys G., Hubrig S., Wolff B., Savanov I., 2006, MNRAS, 372, 286
Kurtz D. W., Elkin V. G., Mathys G., 2007a, MNRAS, 380, 741
Kurtz D. W., Elkin V. G., Mathys G., van Wyk F., 2007b, MNRAS, 381, 1301
Kurtz D. W. et al., 2011, MNRAS, 414, 2550
Landstreet J. D., Mathys G., 2000, A&A, 359, 213
Martinez P., Kauffmann G., 1990, Inf. Bull. Var. Stars, 3507, 1
Martinez P., Kurtz D. W., 1990, Inf. Bull. Var. Stars, 3509, 1
Martinez P., Kurtz D. W., 1992, Inf. Bull. Var. Stars, 3750, 1
Martinez P., Kurtz D. W., Heller C. H., 1990a, MNRAS, 246, 699
Martinez P., Kurtz D. W., Kauffmann G., Jonson A. C., 1990b, Inf. Bull. Var. Stars, 3506, 1
Martinez P., Kurtz D. W., Kauffmann G. M., 1991, MNRAS, 250, 666
Martinez P., Kurtz D. W., Kreidl T. J., Koen C., van Wyk F., Marang F., Roberts G., 1993a, MNRAS, 263, 273
Martinez P., Kurtz D. W., Ashley R., 1993b, Inf. Bull. Var. Stars, 3844, 1
Martinez P., Kurtz D. W., van Wyk F., 1994, MNRAS, 271, 305
Martinez P., Kurtz D. W., Hoffman M. J. H., van Wyk F., 1995, MNRAS, 276, 1435
Martinez P., Koen C., Sullivan D. J., 1998a, MNRAS, 300, 188
Martinez P., Meintjes P., Ratcliff S. J., Engelbrecht C., 1998b, A&A, 334, 606
Mason B. D., Wycoff G. L., Hartkopf W. I., Douglass G. G., Worley C. E., 2001, AJ, 122, 3466
Mathys G., Lanz T., 1992, A&A, 256, 169
Mathys G., Hubrig S., Landstreet J. D., Lanz T., Manfroid J., 1997, A&AS, 123, 353
Mathys G., Kurtz D. W., Elkin V. G., 2007, MNRAS, 380, 181
Matthews J. M., Wehlau W. H., Kurtz D. W., 1987, ApJ, 313, 782
Mkrtichian D. E., Hatzes A. P., Saio H., Shobbrook R. R., 2008, A&A, 490, 1109
Morgan W. W., 1933, ApJ, 77, 330
Murphy S. J., 2012, MNRAS, 422, 665
Murphy S. J., 2014, PhD thesis, Univ. Central Lancashire, UK
Murphy S. J., Shibahashi H., Kurtz D. W., 2013, MNRAS, 430, 2986
Niemczura E. et al., 2015, MNRAS, 450, 2764
North P., 1985, A&A, 148, 165
Paxton B. et al., 2013, ApJS, 208, 4
Perryman M. A. C., ESA eds., 1997, ESA SP-1200, The HIPPARCOS and TYCHO Catalogues. ESA, Noordwijk
Raskin G. et al., 2011, A&A, 526, A69
Renson P., Manfroid J., 2009, A&A, 498, 961
Roeser S., Demleitner M., Schilbach E., 2010, AJ, 139, 2440
Ryabchikova T., Piskunov N., Kochukhov O., Tsymbal V., Mittermayer P., Weiss W. W., 2002, A&A, 384, 545
Ryabchikova T., Nesvacil N., Weiss W. W., Kochukhov O., Stütz C., 2004, A&A, 423, 705
Saio H., 2005, MNRAS, 360, 1022
Smith K. C., 1996, Ap&SS, 237, 77
Sousa S. G., Cunha M. S., 2008, MNRAS, 386, 531
Still M., Barclay T., 2012, Astrophysics Source Code Library, record ascl:1208.004
Stoehr F. et al., 2008, in Argyle R. W., Bunclark P. S., Lewis J. R., eds, ASP Conf. Ser. Vol. 394, Astronomical Data Analysis Software and Systems XVII. Astron. Soc. Pac., San Francisco, p. 505
Stępień K., 2000, A&A, 353, 227
Telting J. H. et al., 2014, Astron. Nachr., 335, 41
Torres G., Andersen J., Giménez A., 2010, A&AR, 18, 67
Watson C. L., Henden A. A., Price A., 2006, Soc. Astron. Sci., 25, p. 47
Wolff S. C., 1983, NASA SP-463: The A-type Stars: Problems and Perspectives. NASA, Washington, DC
Zacharias N., Finch C. T., Girard T. M., Henden A., Bartlett J. L., Monet D. G., Zacharias M. I., 2013, AJ, 145, 44

This paper has been typeset from a TEX/LATEX file prepared by the author.